SOURCE AREAS FOR SCALARS AND SCALAR FLUXES

H. P. SCHMID

Division of Climate Research, Dept. of Geography, Swiss Federal Institute of Technology, Zürich, Switzerland

(Received in final form 6 May, 1993)

Abstract. The spatial resolution of meteorological observations of scalars (such as concentrations or temperature) and scalar fluxes (e.g., water-vapour flux, sensible heat flux) above inhomogeneous surfaces is in general not known. It is determined by the surface area of influence or *source area* of the sensor, which for sensors of quantities that are subject to turbulent diffusion, depends on the flow and turbulence conditions.

Functions describing the relationship between the spatial distribution of surface sources (or sinks) and a measured signal at height in the surface layer have been termed the *footprint function* or the *source weight function*. In this paper, the source area of level P is defined as the integral of the source weight function over the smallest possible domain comprising the fraction P of the total surface influence reflected in the measured signal. Source area models for scalar concentration and for passive scalar fluxes are presented. The results of the models are presented as characteristic dimensions of the $P = 50\%$ source areas (i.e., the area responsible for 50% of the surface influence): the maximum source location (i.e., the upwind distance of the surface element with the maximum-weight influence), the near and the far end of the source area, and its maximal lateral extension. These numerical model results are related directly to non-dimensional surface-layer scaling variables by a non-linear least squares method in a parameterized model which provides a user-friendly estimate of the surface area responsible for measured concentrations or fluxes. The source area models presented here allow conclusions to be made about the spatial representativeness and the localness (these terms are defined in the text) of flux and concentration measurements.

1. Introduction

In recent years the interests and efforts of boundary-layer meteorologists have increasingly been directed towards problems of surface-atmosphere interaction over spatially inhomogeneous regions. At the base of most such problems lies the fundamental difficulty that the well-established homogeneous surface-layer relationships used to describe turbulent exchange of heat, mass and momentum collapse in regions of inhomogeneity. Clearly, however, the atmospheric implications of surface inhomogeneity are primarily a problem of scale and resolution: relatively large-scale (and geometrically simple) surface inhomogeneities can often be resolved well by models or observation networks, and thus the varying regimes of exchange processes over different surface patches can be described and modelled relatively accurately. As a result, our physical understanding of phenomena such as sea-breeze systems, the urban heat island or the development of internal boundary layers is quite advanced and for many purposes sufficient.

The detailed resolution of individual patches comprising an inhomogeneous

Boundary-Layer Meteorology **67**: 293–318, 1994.

surface of a fine texture (e.g., urban areas, agricultural patchwork, etc.) on the other hand is in most cases impractical, or even impossible. The spatial resolution of observations is in general not known at all or only vaguely guessed at. It is determined by the "field of view" or the *surface area of influence* of the sensor. Whereas the effective field of view of surface radiation sensors can (to first order) easily be evaluated by geometrical considerations (see Schmid *et al.*, 1991), the problem is not so simple for sensors of quantities that are subject to turbulent diffusion: the surface-"field of view" (in a figurative sense) is determined by turbulent diffusion itself and is constantly changing in size and position, depending on wind direction and speed and on other characteristics of the flow.

Due to these difficulties (and the need to obtain and interpret observations nevertheless), a number of studies have recently emerged that address the relationship between the spatial distribution of surface sources (or sinks) and a measured signal at height in the surface layer (e.g., Gash, 1986; Schmid and Oke, 1988, 1990; Schuepp *et al.*, 1990; Leclerc and Thurtell, 1990; Wilson and Swaters, 1991; Horst and Weil, 1992a,b; Leclerc *et al.*, 1992). These studies focus on a common problem (originally discussed by Pasquill, 1972), but their separate approaches lead to different instruments of solution that are not applicable interchangeably. For clarity, these may be divided into two classes: the *source weight function* or *footprint* (e.g. Schuepp *et al.*, 1990; Leclerc and Thurtell, 1990; Horst and Weil, 1992a,b; Leclerc *et al.*, 1992) and the "effective fetch" or *source area* (Gash, 1986; Schmid and Oke, 1990; Horst and Weil, 1992a,b). The *source area* can be interpreted as the integral of the *source weight function* over a specified domain (both these terms are defined rigorously in Section 2). Wilson and Swaters (1991) introduce the "distribution of contact distance" which is roughly similar to the source weight, but contains mixed-layer as well as surface-layer diffusion effects. Among these studies, both Eulerian and Lagrangian frameworks are used, but Horst and Weil (1992a) show that they are equivalent for source weight calculations that are confined to the surface layer.

Some of these papers refer to the diffusion of scalars (such as heat, water vapour or other atmospheric admixtures) and their concentration, others to the fluxes of scalars or to both, and Schmid and Oke (1990) do not distinguish between concentrations and fluxes with sufficient emphasis (as has been pointed out by Horst and Weil, 1992a). In addition, it is felt that the terms *footprint* and *source area* are used rather loosely and inconsistently in this group of papers, which can easily lead to misconceptions and confusion. At the *10th Symposium on Turbulence and Diffusion* (AMS, 1992; Portland, Oregon), the validity of the term "footprint" was questioned, since it suggests an incorrect causal relationship (M. Roth, 1992; personal communication). In the following, the term *source weight function* (Schmid and Oke, 1988) will be used instead of *footprint function*, due to its more descriptive quality.

The purpose of the present work is to extend the concepts presented in the above contributions and to offer a clear terminology and notation.

2. Source Weight Functions and Source Areas

The distribution of a diffusing quantity in the atmosphere can be described by the integral equation of diffusion (Pasquill and Smith, 1983):

$$\eta(\mathbf{r}) = \int_{\mathcal{R}} Q_\eta(\mathbf{r}') \cdot f(\mathbf{r} - \mathbf{r}') - \mathrm{d}\mathbf{r}' , \tag{1}$$

where η is the value of the quantity at point $\mathbf{r}$, originating from the source with strength Q_η at $\mathbf{r}'$, f is the probability transfer function between $\mathbf{r}$ and $\mathbf{r}'$ and the convolution is performed over domain $\mathcal{R}$. If the source strength distribution is confined to the surface ($z = z_0$) and diffusion parallel to the mean wind direction (i.e., along the x-axis) is neglected, (1) may be written for an observation point at $(0, 0, z_m)$:

$$\eta(0, 0, z_m) = \int_{-\infty}^{\infty} \int_{-\infty}^{x} Q_\eta(x, y, z = z_0) \cdot f(-x, -y, z_m - z_0) \cdot \mathrm{d}x \cdot \mathrm{d}y . \tag{2}$$

In this case, $f(-x, -y, z_m - z_0)$ relates the value of η at $(0, 0, z_m)$ to the source distribution on the ground and will henceforth be referred to as the *source weight function*. The functional value of the source weight can be interpreted as the relative weight of a given source (at x_S, y_S, z_0, say) to contribute to the value of δ at an observation or reference point. The source weight is thus dependent on the separation distance between the source and the reference point. Its functional form, however, is determined by the diffusion and transport properties relevant for the distribution of η, and on the nature of η itself, as can easily be seen by considering a point source of unit strength at (x_S, y_S, z_0), such that

$$Q_\eta(x, y, z_0) = Q_{\eta,u} \cdot \delta(x_s - x) \cdot \delta(y_s - y) . \tag{3}$$

Here, $Q_{\eta,u}$ is a constant of unit source strength to ensure dimensional consistency and η is the Dirac-delta distribution function. Thus, if the convolution (2) is performed with (3), the value $\eta(0, 0, z_m)$ is proportional to the source weight function f:

$$\eta(0, 0, z_m) = Q_{\eta,u} \cdot f(-x_s, -y_s, z_m - z_0) . \tag{4}$$

Here η may be any diffusing quantity, but whether it is a scalar or (e.g.) a scalar flux must be reflected in the functional form of f. If the diffusion of η is passive and individual sources are independent of each other, it thus suffices to compute the distribution of η at level z_m due to a surface point source with horizontal separation (x, y), in order to evaluate its source weight function. In an advective situation, most of the output from sources close-by will not have enough time to be diffused up to z_m before being advected past the reference point. Thus, the source weight is small for small separation distances. It will rise to a maximum

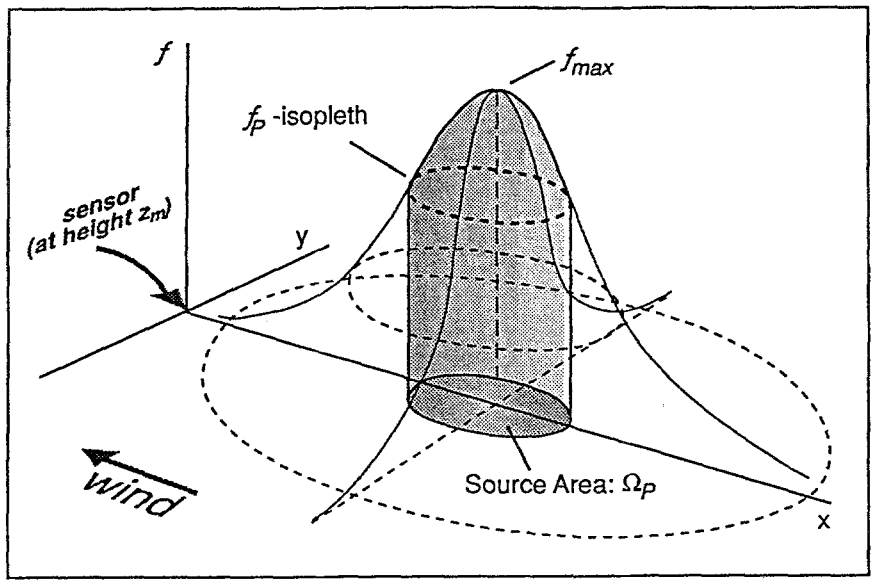

Fig. 1. The source area and its relation to the source weight function. The source weight is small for small separation distances. It will rise to a maximum with increasing distance and then fall off again to all sides as the separation is further increased. The total volume under the source weight function is φ_{tot}. P is the fraction of this volume bounded by the isopleth f_P, and the cylinder surface below it (hatched). The source area of level P, Ω_P, is the area bounded by the normal projection of the isopleth f_p on the x-y-plane. Horizontally homogeneous turbulence is assumed, with the mean wind direction parallel but counter to the x-axis direction.

with increasing distance and then fall off again to all sides as the separation is further increased (see Figure 1 for a schematic illustration). Here, and in the following, horizontally homogeneous turbulence is assumed, with the mean wind direction parallel but counter to the x-axis direction. The latter assumption is equivalent to a reflection of the coordinate system relative to the z-axis and simplifies the notation by placing upwind sources in the $x \geq 0$ semiplane (no negative signs in (4)).

The source weight function provides information about the relative weights of individual point sources. In practice, however, it is often desirable to obtain an estimate of what region of the surface is most efficiently influencing the value of η at height z_m. In other words, one might ask: what is the smallest possible area to be responsible for a given contribution P (half, say: $P = 0.5$) to the value of η at height z_m? (Note that only the specific source weight, i.e. the influence of a given source relative to its source strength, is considered here. In effect, this assumes that the surface is made up of an infinite array of unit point sources of possibly different species).

The smallest such area, Ω_P, was termed the *source area of level P* by Schmid and Oke (1988). It is defined as the area bounded by a source weight function-

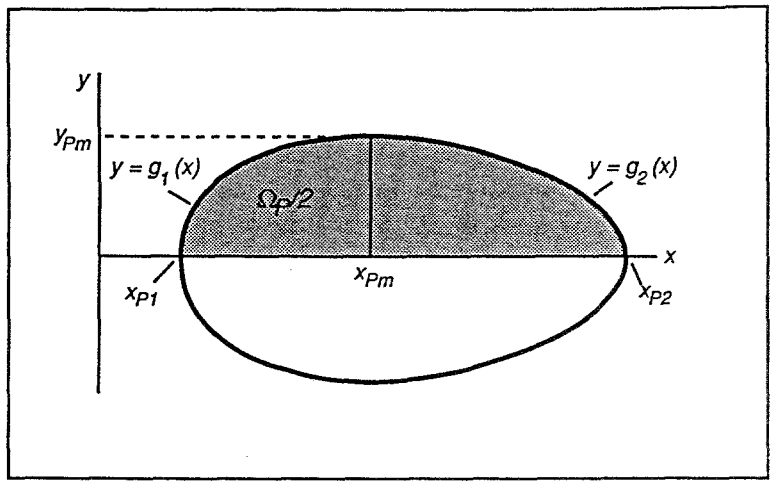

Fig. 2. Schematic illustration of the bounding isopleth for the source area Ω_P. The integration limits for the area bounded by the isopleth are defined in the y-direction by the range $-y_{Pm} \leqslant y \leqslant +y_{Pm}$, where $\pm y_{Pm}$ is the maximal width of the isopleth in positive and negative y-direction respectively; and in the x-direction by the two curves $y = g_1(x)$ and $y = g_2(x)$, defined in the ranges $x_{P1} < x \leqslant x_{Pm}$ and $x_{Pm} \leqslant x \leqslant x_{P2}$ respectively. The inverse of these curves $x = g_{1,2}^{-1}(y)$. If lateral diffusion is Gaussian, symmetry relative to the x-axis can be assumed.

isopleth $f(x, y, z_m - z_0) = f_P$, such that P is the fraction of the total integrated source weight function, φ_{tot}, contained in Ω_P:

$$P = \frac{\varphi_P}{\varphi_{\text{tot}}} = \int_{\Omega_P}\int f(x, y, z_m - z_0) \cdot \mathrm{d}x \cdot \mathrm{d}y \Big/ \int_{-\infty}^{+\infty}\int_{0}^{+\infty} f(x, y, z_m - z_0) \cdot \cdot \mathrm{d}x \cdot \mathrm{d}y \,, \tag{5}$$

where φ_P is the integral of the source weight function over Ω_P. The source area and its relation to the source weight function is illustrated schematically in Figure 1. The source area fraction P is equivalent to the volume under the source weight function, bounded by the isopleth f_P, and the cylinder surface below it.

With (4), Equation (5) reduces to:

$$P = \frac{\varphi_P}{\varphi_{\text{tot}}} = \int_{\Omega_P}\int \eta(x, y, z_m) \cdot \mathrm{d}x \cdot \mathrm{d}y \Big/ \int_{-\infty}^{\infty}\int_{0}^{\infty} \eta(x, y, z_m) \cdot \mathrm{d}x \cdot \mathrm{d}y \,, \tag{6}$$

and Ω_P is bounded by $\eta(x, y, z_m) = \eta_P$, where the vertical separation $(z_m - z_0)$ is denoted in simplified form as z_m.

Figure 2 is a schematic representation of an oval-shaped Ω_P, illustrating the integration limits used to compute φ_P, which can thus be written:

$$\varphi_P = \frac{1}{Q_{\eta,u}} \int_{(-y_{Pm})}^{(+y_{Pm})} \int_{(x=g_1^{-1}(y))}^{(x=g_2^{-1}(y))} \eta(x, y, z_m) \cdot \mathrm{d}x \cdot \mathrm{d}y \tag{7}$$

(see Figure 2 for an explanation of the boundaries).

In this form, the definitions of the source weight function (Equations (2) and (4)) and of the source area (Equations (5) and (6)) appear simple. However, as with all applications of the integral equation of diffusion, to give these equations teeth, the nature of the transfer function, in this case of f, or rather of η, needs to be determined, and therein lies the problem. In the following sections, the source weight and the source area for the concentration of a passive scalar (Section 3) and for the flux of a passive scalar (Section 4) will be presented. If a concentration-source area is considered, the notation of the foregoing equations is adjusted so that η becomes the scalar concentration, C, and the unit point source, $Q_{\eta,u}$, becomes $Q_{C,u}$. In case of a flux-source area, η becomes the vertical flux, F, and the unit point source becomes simply F_u. The approach chosen here is based on K-theory and an analytical solution of the advection-diffusion equation by van Ulden (1978). However, the validity of Equations (4) and (6) is not confined to this particular method.

If K-theory is used, the core of any model for the source weight function or the source area (be it for a scalar concentration or a scalar flux) is formed by the scalar concentration distribution $C(x, y, z)$. Depending on the choice of the functional form of the concentration distribution, and of the shape of the wind-profile, $\bar{u}(z)$, analytical solutions for the source areas of scalars and scalar fluxes, respectively, may be possible. However, the present study employs a surface-layer dispersion model presented by Gryning *et al.* (1987), which by itself cannot be solved analytically, but has the advantage of including thermal stratification and a realistic wind profile. This dispersion model is the same as that used for the scalar source area model (SAM) by Schmid and Oke (1988, 1990), but is extended to include stable stratification here. The determination of $C(x, y, z_m)$ is strongly dependent on the reference height z_m and is further affected by the familiar surface-layer scaling parameters: the Obukhov length, L; the surface roughness length, z_0; the friction velocity, u_*; and the standard deviation of lateral wind speed fluctuations σ_v.

The steps undertaken in the computer implementation of the source area models for scalar concentrations (Scalar source Area Model, SAM) and for scalar fluxes (scalar Flux-Source Area Model, FSAM) are similar. In principle, the distribution of scalar concentration, $C(x, y, z_m)$, (in case of SAM) or of the flux, $F(x, y, z_m)$, for FSAM, due to a unit surface point source, is given for any downwind location (x, y) by a suitable diffusion model. However, due to numerical limitations, these distributions can be computed only for $x \geq x_{\min}$. This minimum separation distance needs to be determined in a preliminary step. The remaining steps to compute the source areas for several values of P can be summarised as follows (again, η

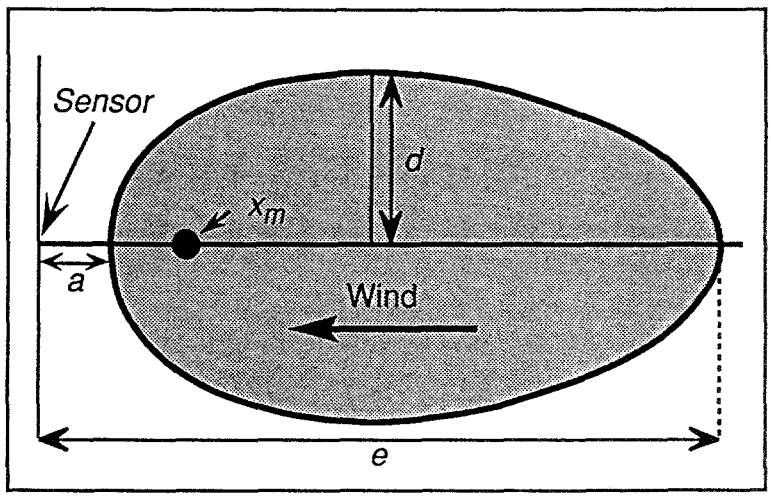

Fig. 3. Characteristic dimensions of the source area. x_m: maximum source location (upwind distance of the surface element with the maximal influence on a given sensor); a: near end; e: far end; and d: maximum lateral half-width of the source area (from Schmid *et al.*, 1991). The size of the area bounded by the isopleth is denoted as Ar, and the upwind distance of the maximum width (d) as x_d. Wherever applicable, the SAM dimensions for a scalar concentration are provided with an index 'c', to distinguish them from the FSAM dimensions of the flux-source area (index 'f').

is equivalent to the source weight distribution and stands for C or for F, as the case may be):

1. The maximum value of the distribution function and its location, $\eta_{\max}$ and x_m is determined by a numerical search.
2. A number of η-values are defined as fractions of $\eta_{\max}$: η_i, for $i = 1, \ldots, n$.
3. The isopleths corresponding to η_i are determined by root-finders and the source weight functions are integrated incrementally between each two successive isopleths to give the P-levels, P_i, corresponding to each isopleth level η_i. The pairs (P_i, η_i) are considered as nodes of a continuous function $\eta = \eta(P)$.
4. The isopleth values corresponding to round decadal-fraction values of P are determined by cubic spline interpolation of the function $\eta = \eta(P)$. The characteristic dimensions of these isopleths are then determined by numerical search methods. Apart from the upwind distance of the maximum source location (x_m), which is computed in step 1 and is independent of P, these dimensions are (see Figure 3): the upwind distance to the near end of the isopleth (a) and to the far end of the isopleth (e), and the maximum lateral half-width of the isopleth (d). In addition, the size of the area bounded by the isopleth is determined (Ar).

3. The Source Area for a Passive Scalar

3.1. SAM-2: THEORY

Following Horst and Weil (1992a), the concentration distribution, $C(x, y, z_m)$, downwind of a unit surface point source of a passively diffusing scalar can be described as:

$$C(x, y, z_m) = Q_{C,u} \cdot \frac{D_y(x, y) \cdot D_z(x, z_m)}{U(x)}, \tag{8}$$

where $Q_{C,u}$ is the unit point source strength, D_y and D_z are the crosswind and vertical concentration distribution functions, respectively and $U(x)$ is the effective speed of plume advection (i.e., the vertical integration, from z_0 to ∞, of the local windspeed times D_z; see e.g., Horst and Weil, 1992a). In (8) and in the following, streamwise diffusion is neglected and the x-axis is chosen to be parallel to the mean wind direction. As indicated by (8), lateral crosswind diffusion and vertical diffusion can be treated independently. Equation (8) is the equivalent of (4) for a passive scalar, so that the scalar concentration-source weight for a reference point at $z = z_m$, and sources at $z = z_0$ and horizontal separation (x, y) is:

$$f_C(x, y, z_m - z_0) = \frac{C(x, y, z_m)}{Q_{C,u}} = \frac{D_y(x, y) \cdot D_z(x, z_m)}{U(x)}. \tag{9}$$

Gryning *et al.* (1987) provided a closed set of equations for $D_y(x, y)$, $D_z(x, z)$ and $U(x)$, dependent on standard surface-layer scaling parameters and based on an analytical solution of the Eulerian advection-diffusion equation by van Ulden (1978) for vertical diffusion, to give:

$$D_z(x, z) = \frac{A}{\bar{z}(x)} \cdot \exp\left\{ - \left(\frac{B \cdot z}{\bar{z}} \right)^s \right\}, \tag{10}$$

where $A = s \cdot \Gamma(2/s)/\Gamma^2(1/s)$ and $B = \Gamma(2/s)/\Gamma(1/s)$ are functions of the shape parameter, s, Γ is the gamma function, and $\bar{z}$ is the mean height of the plume. An equation to determine the shape parameter s can be found in Gryning *et al.* (1987), and a discretized integration of $d\bar{z}/dx$ (see van Ulden, 1978; his equation (16)) has been used to compute $\bar{z}(x)$.

Diffusion in the lateral direction is commonly assumed to be Gaussian, so that $D_y(x, y)$ can be written:

$$D_y(x, y) = \frac{1}{\sqrt{2\pi} \cdot \sigma_y} \cdot \exp\left\{ - \frac{1}{2} \left(\frac{y}{\sigma_y} \right)^2 \right\}. \tag{11}$$

Here σ_y is the standard deviation of the lateral spread and can be related to the plume travel time, x/U, and the standard deviation of lateral wind fluctuations,

σ_v as $\sigma_y \cong \sigma_v \cdot x/U$, if the validity of the short range-limit solution of statistical turbulence theory is accepted for this purpose (see e.g., Pasquill and Smith, 1983).

The scalar concentration-source area is evaluated by substituting (9) into (6) to give:

$$P_C = \frac{\varphi_{P_C}}{\varphi_{\mathrm{tot}C}} = \int_{\Omega_{P_C}} \int \frac{D_y(x,y) \cdot D_z(x,z_m)}{U(x)} \cdot \mathrm{d}x \cdot \mathrm{d}y \Big/ \int_{-\infty}^{\infty} \int_0^{\infty} \frac{D_y(x,y) \cdot D_z(x,z_m)}{U(x)} \cdot \mathrm{d}x \cdot \mathrm{d}y \,. \tag{12}$$

The subscript C is included in P_C and $\varphi_{\mathrm{tot}C}$, to indicate the scalar concentration-source area.

At this point it is convenient to consider the evaluation of φ_{P_C} and $\varphi_{\mathrm{tot}C}$ separately. Since $\int_{-\infty}^{\infty} D_y \cdot \mathrm{d}y = 1$, the integration of $\varphi_{\mathrm{tot}C}$ can be simplified to

$$\varphi_{\mathrm{tot}C} = \frac{1}{Q_{C,u}} \int_0^{\infty} D_z(x, z_m)/U(x) \cdot \mathrm{d}x \,. \tag{13}$$

The integrand of (13) expresses the ratio of vertical diffusion to advection of C. In stable conditions, this ratio increases with increasing x, whereas it approaches a limit of zero for $x \to \infty$ in unstable conditions (Horst, 1993; personal communication). Thus (13) converges to a finite value only in unstable conditions. However, if lateral diffusion is taken into account, the source weight of C approaches zero for $x \to \infty$ or $y \to \pm\infty$ (at least within the ranges of stability and cross-wind turbulence intensities used in this study; see below). Because of this difficulty, an alternative definition of the total source area for scalar concentration is employed for SAM-2: $\varphi_{\mathrm{tot}C}$ is interpreted as an effective total source area and is approximated by integrating the C-source weight function to an isopleth of 1% of the maximum. This approximation implies that sources outside this 1% limit are insignificant for determination of the concentration at the reference point.

The integration of φ_{P_C} involves the determination of the y-dependent boundaries in $x(x = g_{C,1,2}^{-1}(y)$, where the subscript C indicates the boundary for a scalar concentration-source area), as described in Figure 2 and Equation (7) and symmetry relative to the x-axis can be assumed. In practice, the inversion of the functions $g_{C,1,2}$ involves a numerical search procedure. The computer implementation of this update of the scalar-source area model of Schmid and Oke (1990), with an extension to include stable stratification (SAM-2) follows the procedure outlined at the end of Section 2. The model is coded in FORTRAN and draws on the subroutine libraries published by Press *et al.* (1986) and Beljaars *et al.* (1989).

3.2. SAM-2: RESULTS

The form of the relationship between the modelled source area dimensions and the input variables was evaluated by a large number of SAM-2 runs in a sensitivity

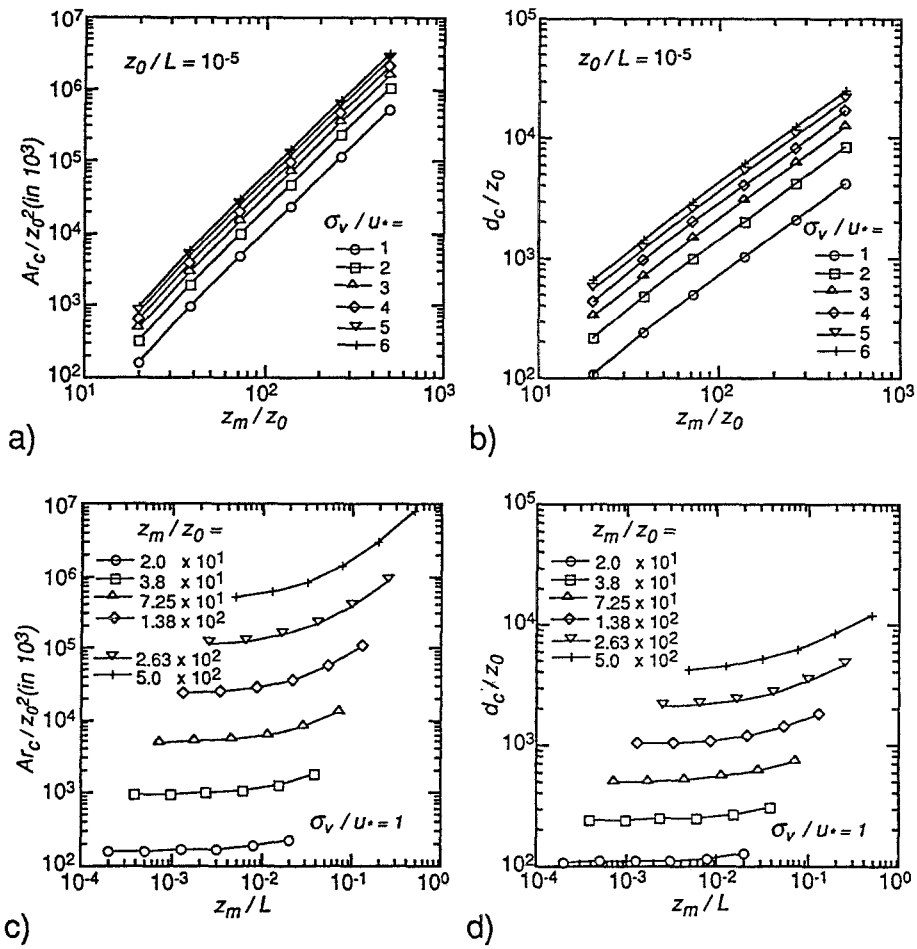

Fig. 4(a–d).

test for the wide range of input values that can be expected in the atmospheric surface layer. If the source area dimensions described in Figure 3 are scaled by z_0 (z_0^2 in the case of the area, Ar_c), the sensitivity test shows clearly that all dimensions are dependent on the non-dimensional variables z_m/z_0 (indicating the measurement height above the roughness elements) and z_m/L (indicating the strength of buoyancy at the reference height), but only the crosswind dimension, d_c, and the area, Ar_c, are also dependent on σ_v/u_*, the strength of lateral wind fluctuations. The resulting normalised dimensions are presented in Figure 4a–h (stable conditions) and Figure 5a–h (unstable conditions) for the scalar concentration-source area with $P = 0.5$ (i.e. the 50% influence source area).

The dependence of Ar_c/z_0^2 and d_c/z_0 on the magnitude of crosswind turbulence

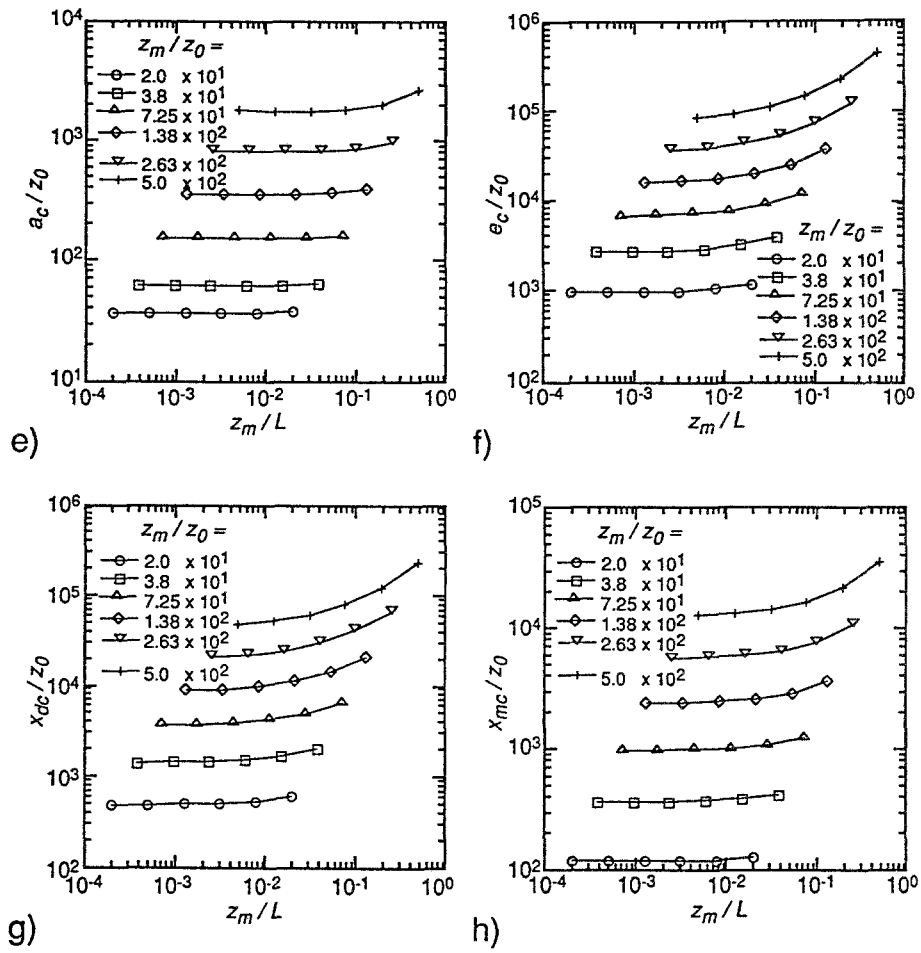

Fig. 4. Dependence of the normalised characteristic dimensions of the scalar-concentration-source area (SAM-2) on the non-dimensional input variables, stable conditions: (a) dependence of the area size on measurement height; (b) dependence of the largest lateral extension on measurement height; stability dependence of (c) the area size, (d) the largest lateral extension, (e) the near upwind boundary, (f) the far upwind/boundary, (g) the upwind distance of the largest lateral extension, and (h) the maximum source location. See Figure 3 for a schematic illustration of these dimensions.

(σ_v/u_*) is linear, in accordance with the linear model of σ_y used in this application. The nearly straight lines of the Ar_c/z_0^2 and d_c/z_0 dependence on z_m/z_0 in the log-log representation of Figures 4a,b and 5a,b suggest a positive power-law relationship between the measurement height and these dimensions. Corresponding plots for the other isopleth dimensions exhibit a similar relationship and are therefore not shown here. In comparison to the measurement height, the dependence on stability (z_m/L) is much weaker, and does not suggest a straightforward power-law relation (Figures 4c–h and 5c–h).

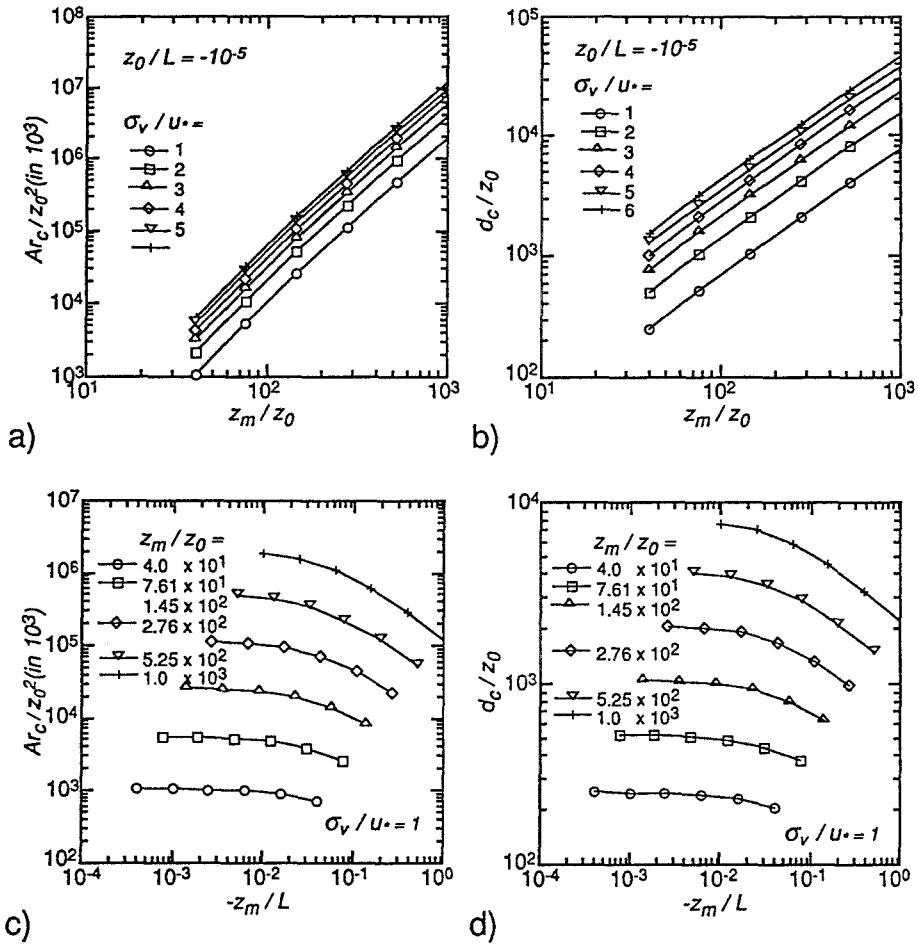

Fig. 5(a–d).

The forms in which the normalised source area dimensions depend on non-dimensional variables, as suggested in these model runs, are exploited in a non-linear parameterisation scheme presented in Section 5.

4. The Source Area for a Scalar Flux

4.1. FSAM: THEORY

Before the source area for a scalar flux can be computed, the source weight function for a scalar flux needs to be considered. An expression for this function is developed following Horst and Weil (1992a).

Using K-theory, the vertical flux of C, F, is expressed (using (8)) as

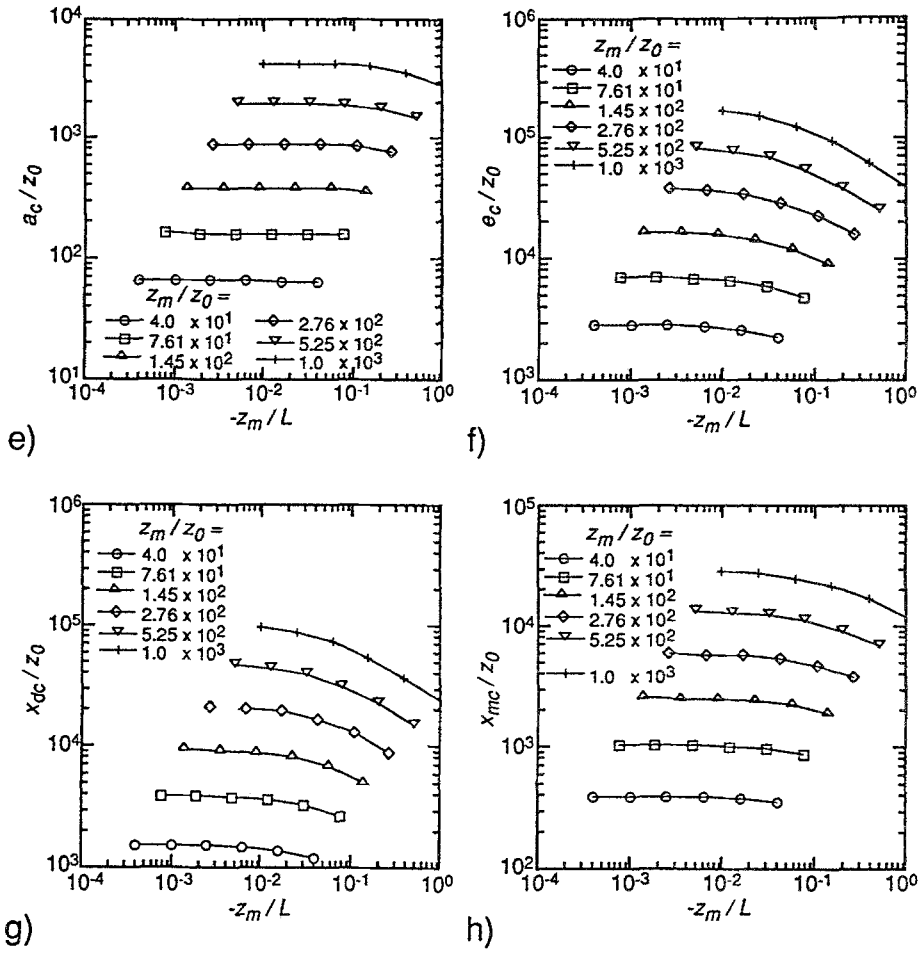

Fig. 5. Same as Figure 4, for SAM-2 in unstable conditions.

$$F(x, y, z) = -K_C(z) \cdot \frac{\partial C}{\partial z} = -K_C(z) \cdot Q_{C,u} \cdot \frac{D_y}{U} \cdot \frac{\partial D_z}{\partial z}$$

$$= D_y(x, y) \cdot \overline{F^y}(x, z)\,, \tag{14}$$

where $K_C(z)$ is an eddy diffusivity and $\overline{F^y}$ is the crosswind integrated flux. Equations (8) and (14) imply that diffusion in the vertical and crosswind directions can be treated independently also for a scalar flux.

The crosswind integrated flux $\overline{F^y}$ is related to the crosswind integrated concentration $\overline{C^y}$ and the mean wind speed profile $\bar{u}(z)$ through the two-dimensional advection diffusion equation:

$$\bar{u}(z) \cdot \frac{\partial}{\partial x} \overline{C^y} = -\frac{\partial}{\partial z} \overline{F^y} \,. \tag{15}$$

This equation may be integrated and the vertical flux at level z_m is expressed as:

$$\overline{F^y}(x, z_m) = \overline{F^y}(x, z_0) - \int_{z_0}^{z_m} \bar{u}(z) \cdot \frac{\partial}{\partial x} \overline{C^y}(x, z) \cdot \mathrm{d}z \,. \tag{16}$$

Applying a boundary condition of a crosswind integrated unit point source, $\overline{F_u^y}$, at ground level such that $\overline{F^y}(x, z_0) = \overline{F_u^y} \cdot \delta(x)$, this equation is reduced for $x > 0$ to:

$$\overline{F^y}(x > 0, z_m) = -\int_{z_0}^{z_m} \bar{u}(z) \cdot \frac{\partial}{\partial x} \overline{C^y}(x, z) \cdot \mathrm{d}z \,. \tag{17}$$

With (4), (14), (16) and (17), the two-dimensional flux-source weight function $f_F(x, y, z_m z_0)$ becomes:

$$f_F(x, y, z_m - z_0) = \frac{F(x, y, z_m)}{F_u} = \frac{1}{F_u} \cdot [\overline{F^y}(x, z_0) + \overline{F^y}(x > 0, z_m)] \cdot \cdot D_y(x, y) \,. \tag{18}$$

The dependence of the crosswind integrated form of this function on measurement height, surface roughness and stability is analysed extensively by Horst and Weil (1992a).

With this definition of the flux-source weight function and with Equation (6), the flux-source area Ω_{P_F}, of level P_F, is formulated as the area bounded by an isopleth of $F(x, y, z_m - z_0) = F_P$, such that P_F is the fraction of the total integrated source weight function, φ_{tot_F}, contained in Ω_{P_F}:

$$P_F = \frac{\varphi_{P_F}}{\varphi_{\mathrm{tot}_F}} = \int_{\Omega_{P_F}} \int F(x, y, z_m) \cdot \mathrm{d}x \cdot \mathrm{d}y \Big/ \int_{-\infty}^{\infty} \int_{0}^{\infty} F(x, y, z_m) \cdot \mathrm{d}x \cdot \mathrm{d}y \,, \tag{19}$$

where φ_{P_F} is the integral of the source weight function over Ω_P. This is in analogy to the definition of the scalar concentration-source area (see Figure 1 for a schematic illustration). Again, it is useful to consider φ_{tot_F}, and φ_{P_F} separately.

The total integrated source weight function, φ_{tot_F}, is evaluated as:

$$\varphi_{\mathrm{tot}_F} = \frac{1}{F_u} \cdot \int_{-\infty}^{\infty} \int_{0}^{\infty} F(x, y, z_m) \cdot \mathrm{d}x \cdot \mathrm{d}y = \frac{1}{F_u} \cdot \int_{0}^{\infty} \overline{F^y}(x, z_m) \cdot \mathrm{d}x \,. \tag{20}$$

With (16) this equation becomes

$$\varphi_{\mathrm{tot}_F} = \frac{1}{F_u} \cdot \left\{ \int_0^{\infty} \left[\overline{F^y}(x, z_0) - \int_{z_0}^{z_m} \bar{u}(z) \cdot \frac{\partial}{\partial x} \overline{C^y}(x, z) \cdot \mathrm{d}z \right] \cdot \mathrm{d}x \right\}, \tag{21}$$

and can be simplified to

$$\varphi_{\mathrm{tot}_F} = \frac{1}{F_u} \cdot \left\{ \int_0^{\infty} \overline{F^y}(x, z_0) \cdot \mathrm{d}x - \int_{z_0}^{z_m} \bar{u}(z) \cdot \overline{C^y}(x, z) \Big|_{x=0}^{x=\infty} \cdot \mathrm{d}z \right\}. \tag{22}$$

The term inside the brackets is the areally integrated flux of C through the horizontal plane $z = z_m$. Since the only source of C is the surface emission flux, expressed as $\overline{F^y}(x, z_0) = \overline{F_u^y} \cdot \delta(x)$, mass continuity dictates that the second term inside the bracket be zero (note that in (21) the integration in x is over the closed interval $[0, \infty]$, including $x = 0$), whereas the first term integrates to F_u. Thus,

$$\varphi_{\mathrm{tot}_F} = 1 . \tag{23}$$

This representation of the total flux-source area implies that no sources or sinks of C exist in the layer below z_m other than the surface emission flux due to a point source and that the volume of air where diffusion takes place is in a condition of steady state. In other words: what is injected into the atmosphere at the surface, must eventually pass through level z_m. This assumption is equivalent to the existence of a constant flux layer above a surface with uniform emission flux.

With (23), (19) reduces to

$$P_F = \frac{\varphi_{P_F}}{\varphi_{\mathrm{tot}_F}} = \frac{1}{F_u} \cdot \int_{\Omega_{P_F}} \int F(x, y, z_m) \cdot \mathrm{d}x \cdot \mathrm{d}y . \tag{24}$$

For any value of P_F, other than $P_F = 1$, the boundary of Ω_{P_F} is limited to $x > 0$, and thus, (24) can be written with (17) and (18):

$$P_F = \frac{1}{F_u} \cdot \int_{\Omega_{P_F}} \int \left[- \int_{z_0}^{z_m} \bar{u}(z) \cdot \frac{\partial}{\partial x} \overline{C^y}(x, z) \cdot \mathrm{d}z \cdot D_y(x, y) \right] \cdot$$

$$\cdot \mathrm{d}x \cdot \mathrm{d}y; \qquad \text{for } x > 0 . \tag{25}$$

Again, the integration domain, Ω_{P_F}, is explained and illustrated in Figure 2. Thus, it is useful to take advantage of the symmetry with respect to the x axis of the (Gaussian) D_y-distribution, and (25) may be written, using Leibnitz's rule:

$$P_F = -\frac{2}{F_u} \cdot \int_0^{y_{PFm}} \int_{z_0}^{z_m} \bar{u}(z) \cdot C(x, y, z) \Big|_{x = g_{F,1}^{-1}(y)}^{x = g_{F,2}^{-1}(y)} \cdot \mathrm{d}z \cdot \mathrm{d}y . \tag{26}$$

Here, $x = g_{F,1,2}^{-1}(y)$ are the inverted boundary functions for the flux-source area, which are determined by a numerical root-finder routine for the F-level corresponding to P_F based on Equation (17).

Equation (26) indicates that the value of the flux-source weight function at any particular point does not have to be evaluated for the integration of the flux-

source area. However, it needs to be computed for the determination of the integration limits, i.e., for the values of the inverse functions $x = g^{-1}_{F,1,2}(y)$ and of y_{Pm}. Apart from this simplification for the x-integration of the flux-source area, the steps undertaken in the computer implementation of the source area models for scalar concentrations (SAM-2) and for scalar fluxes (FSAM) are similar (see the end of Section 2).

4.2. FSAM: RESULTS

Since the flux-source area model (FSAM) is based on the same solution of the advection-diffusion equation as SAM-2, the appropriately normalised flux-source area dimensions (with subscript f to denote the flux-source area) are also dependent on the non-dimensional variables z_m/z_0, z_m/L, and, for d_f/z_0 and Ar_f/z_0^2, on σ_v/u_*. A similar sensitivity test as described in Section 3.2 for SAM-2 was performed for FSAM. Due to numerical constraints in the (vertical) integration over (horizontal) gradients of concentration in order to evaluate the flux, the range of input values that led to successful FSAM runs was more limited than in the sensitivity test of SAM-2. As a result of these limitations, the permissible stability variable had to be constrained to values of $z_m/L \leq 10^{-1}$.

The results of the FSAM evaluations are presented in Figure 6a–h (stable stratification) and Figure 7a–h (unstable conditions), using a similar format as in Figures 4 and 5. The shapes of the relationships between the normalised FSAM dimensions and the input variables exhibit a considerable similarity to the results of SAM-2 for the scalar-source areas. In absolute value, however, the FSAM dimensions are generally found to be smaller than the SAM-2 dimensions by almost an order of magnitude (except in the case of a/z_0, where the SAM-2 value is slightly smaller than the corresponding FSAM dimension).

The good qualitative agreement between source areas for fluxes and concentrations also suggests the use of similar parameterisation schemes for SAM-2 and FSAM, as described in the following section.

5. Parameterized Models of Source Areas for Scalars and Scalar Fluxes

Each run of the source area models involves a large number of floating point operations and thus takes up considerable computing time and costs (for a run of FSAM on a VAX 9000-420 with two processors approximately five minutes of CPU time is needed, depending on the choice of input parameters). For this reason, the normalised dimensions of the $P = 0.5$ source areas as computed in the sensitivity tests described in Sections 3.2 and 4.2 were related directly to the non-dimensional parameters z_m/z_0, z_m/L, and σ_v/u_* (see Section 2).

For these parameterisations of SAM-2 and FSAM, the non-dimensional input values were varied over the following ranges of commonly observed surface-layer conditions:

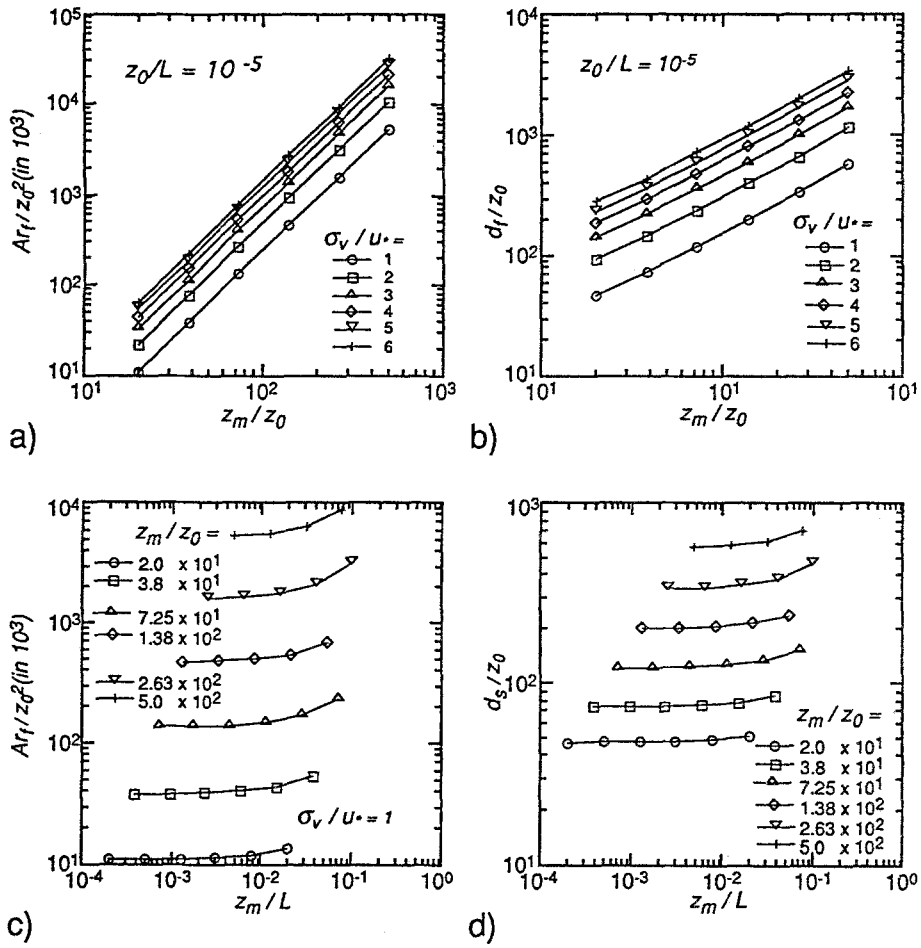

Fig. 6(a–d).

for stable conditions ($z_m/L > 0$),

$$2.0 \cdot 10^1 \leqslant z_m/z_0 \leqslant 5.0 \cdot 10^2$$

$$2.0 \cdot 10^{-4} \leqslant z_m/L \leqslant 1.0 \cdot 10^{-1}$$

$$1.0 \leqslant \sigma_v/u_* \leqslant 6.0$$

and for unstable conditions ($z_m/L < 0$),

$$4.0 \cdot 10^1 \leqslant z_m/z_0 \leqslant 1.0 \cdot 10^3$$

$$4.0 \cdot 10^{-4} \leqslant -z_m/L \leqslant 1.0$$

$$1.0 \leqslant \sigma_v/u_* \leqslant 6.0\,.$$

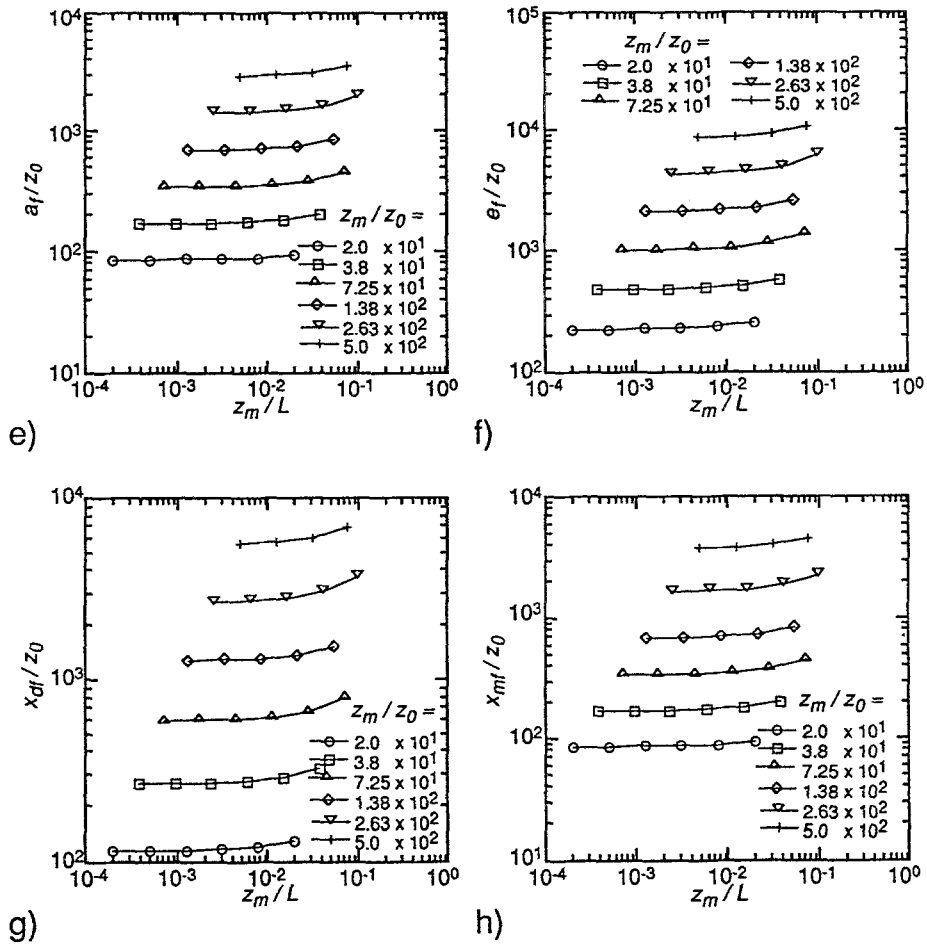

Fig. 6. Same as Figure 4, for FSAM in stable conditions.

Within these ranges the additional condition $10^{-5} \leq |z_o/L| \leq 10^{-3}$ was observed (see Figures 4 to 7).

Adequate mathematical relationships between the input variables and the model output were determined graphically (Figures 4 to 7), and a best fit was found by a non-linear least squares method, based on a modified Levenberg–Marquardt algorithm (IMSL Inc., statistics library, see also Press *et al.*, 1986). In reference to a previously published parameterised (scalar concentration) source area model (mini-SAM, by Schmid and Oke, 1990) the resulting set of equations is termed mini-*SAM-2* for the scalar concentration-source area model and mini-*FSAM* for the scalar flux-source area model. For each of the six normalised mini-SAM-2 and mini-FSAM dimensions, D_N, the regression was performed separately for stable

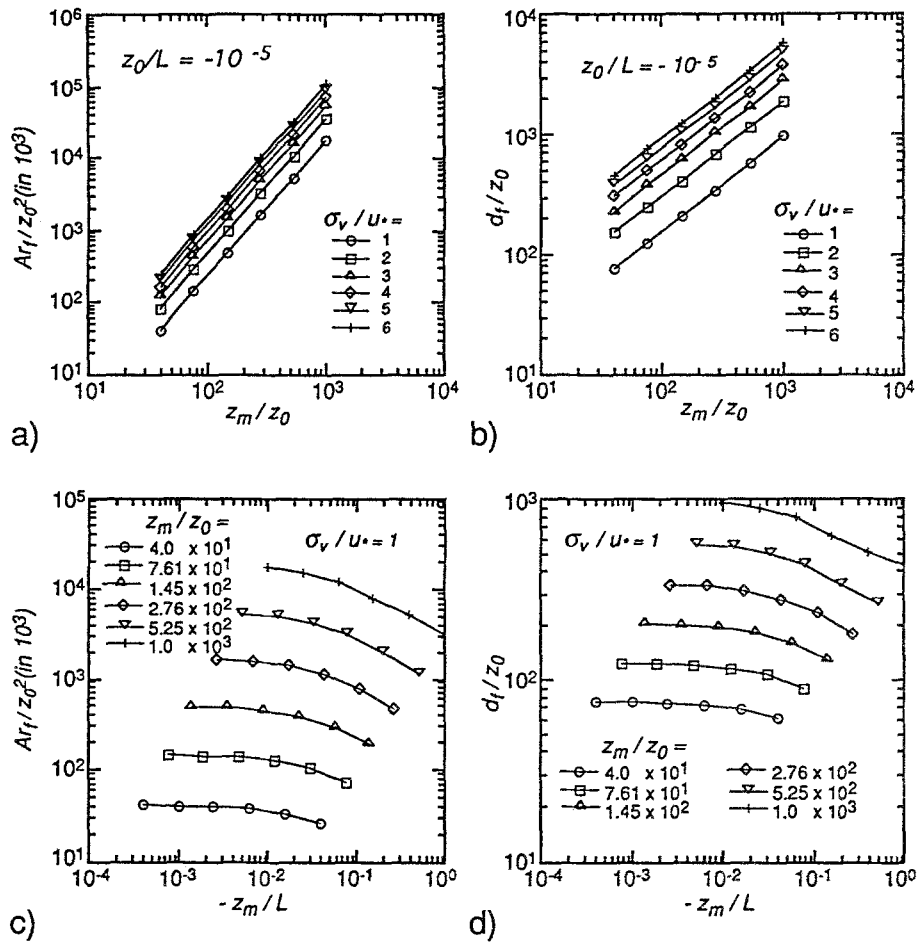

Fig. 7(a–d).

and unstable conditions, resulting in 24 sets of parameters, α_i ($i = 1, 5$), referring to two types of equation:

$$D_N = \alpha_1 \cdot (z_m/z_0)^{\alpha_2} \cdot \exp\{\alpha_3 \cdot (z_m/L)^{\alpha_4}\} \cdot (\sigma_v/u_*)^{\alpha_5}, \tag{27a}$$

$$D_N = \alpha_1 \cdot (z_m/z_0)^{\alpha_2} \cdot (1 - \alpha_3 \cdot z_m/L)^{\alpha_4} \cdot (\sigma_v/u_*)^{\alpha_5}. \tag{27b}$$

The individual parameter values are listed in Tables I and II for mini-SAM-2 and in Tables V and VI for mini-FSAM.

The mini-SAM-2 (or mini-FSAM) estimate of a particular source area dimension is readily obtained by first choosing the appropriate table for the given stability conditions. Each line of the tables refers to the normalised source area dimension indicated in the first column. The second column gives the equation number to

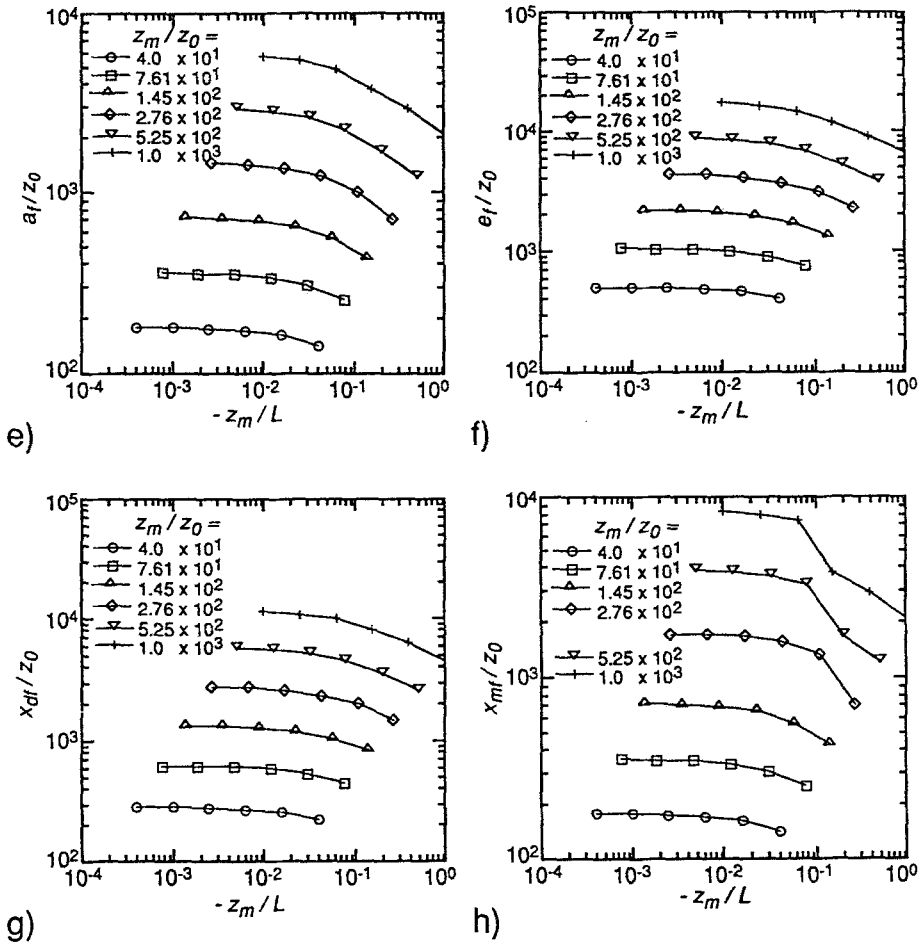

Fig. 7. Same as Figure 4, for FSAM in unstable conditions.

TABLE I

Parameter values for the 50% passive scalar source area model (SAM-2) parameterisation, stable stratification (to be used in Equation 27a)

Normalised dimension	Reference equation	α_1	α_2	α_3	α_4	α_5
a_c/z_0	27a	0.773	1.24	0.957	1.25	0
e_c/z_0	27a	30.4	1.23	2.60	0.452	0
d_c/z_0	27a	4.31	1.07	1.69	0.397	1
x_{dc}/z_0	27a	15.7	1.25	2.49	0.449	0
x_{mc}/z_0	27a	4.30	1.28	1.74	0.688	0
Ar_c/z_0^2	27a	$0.203 \cdot 10^3$	2.28	4.38	0.408	1

TABLE II

Parameter values for the 50% passive scalar source area model (SAM-2) parameterisation, unstable stratification (to be used in Equations 27a, b)

Normalised dimension	Reference equation	α_1	α_2	α_3	α_4	α_5
a_c/z_0	27a	0.853	1.23	0.441	1	0
e_c/z_0	27b	40.4	1.22	15.5	−0.548	0
d_c/z_0	27b	5.73	1.05	16.8	−0.458	1
x_{dc}/z_0	27b	21.3	1.23	16.9	−0.517	0
x_{mc}/z_0	27b	5.37	1.25	5.96	−0.472	0
Ar_c/z_0^2	27b	$0.405 \cdot 10^3$	2.25	16.0	−1.03	1

TABLE III

Validation statistics* for the parameterisation of the passive scalar source area model (SAM-2), stable stratification (Equation 27a)

	a_c/z_0	e_c/z_0	d_c/z_0	x_{dc}/z_0	x_{mc}/z_0	Ar_c/z_0^2
Number of runs (n)	36	36	216	36	36	216
Coeff. of determination (r^2)	0.9998	0.9999	0.9998	0.9999	0.9998	1.0000
Index of agreement (d)	0.9999	1.0000	1.0000	1.0000	0.9999	1.0000
rel. $RMSE_{tot}$ [%]	1.76	1.95	1.97	2.00	2.15	2.27
rel. $RMSE_{sys}$ [%]	0.44	0.64	0.21	0.65	0.96	0.10
rel. $RMSE_{unsys}$ [%]	1.70	1.84	1.97	1.89	1.92	2.27

* Definition of statistics used (for a detailed description, see Wilmott, 1981):

r^2: coefficient of determination (i.e., the square of Pierson's product-moment correlation coefficient); $0 \leq r^2 \leq 1$

d: index of agreement (i.e., the degree to which the modelled deviations about the modelled mean correspond both in sign and magnitude to the parameterised deviations, where the modelled mean is considered error-free); $0 \leq d \leq 1$

rel. RMSE: standard error or difference, relative to the modelled mean (where $RMSE_{tot}$: RMSE between modelled and parameterised values; $RMSE_{sys}$: RMSE between regressed and modelled values, where a linear least squares regression is used; $RMSE_{unsys}$: RMSE between regressed and parameterised values; $RMSE_{tot}^2 = RMSE_{sys}^2 + RMSE_{unsys}^2$)

TABLE IV

Validation statistics for the parameterisation of the passive scalar source area model (SAM-2), unstable stratification (Equations 27a and b). For a description of the statistics used, see Table III

	a_c/z_0	e_c/z_0	d_c/z_0	x_{dc}/z_0	x_{mc}/z_0	Ar_c/z_0^2
Number of runs (n)	36	36	216	36	36	216
Coeff. of determination (r^2)	0.9998	0.9999	1.0000	0.9999	0.9999	1.0000
Index of agreement (d)	0.9999	1.0000	1.0000	1.0000	1.0000	1.0000
rel. $RMSE_{tot}$ [%]	1.74	1.58	1.89	1.47	1.60	1.27
rel. $RMSE_{sys}$ [%]	0.62	0.71	0.29	0.73	0.88	0.20
rel. $RMSE_{unsys}$ [%]	1.63	1.41	1.84	1.27	1.34	1.25

TABLE V

Parameter values for the passive scalar flux-source area model (FSAM) parameterisation, stable stratification (to be used in Equations 27a)

Normalised dimension	Reference equation	α_1	α_2	α_3	α_4	α_5
a_f/z_0	27a	3.28	1.09	3.53	1.05	0
e_f/z_0	27a	10.1	1.08	3.84	1.07	0
d_f/z_0	27a	4.07	0.790	2.97	0.977	1
x_{df}/z_0	27a	4.84	1.13	3.83	1.10	0
x_{mf}/z_0	27a	1.58	1.25	2.91	1.02	0
Ar_f/z_0^2	27a	51.3	1.86	7.29	1.05	1

TABLE VI

Parameter values for the 50% passive scalar flux-source area model (FSAM) parameterisation, unstable stratification (to be used in Equation 27b)

Normalised dimension	Reference equation	α_1	α_2	α_3	α_4	α_5
a_f/z_0	27b	2.79	1.11	14.1	−0.399	0
e_f/z_0	27b	8.54	1.11	12.8	−0.390	0
d_f/z_0	27b	3.25	0.832	28.2	−0.272	1
x_{df}/z_0	27b	4.29	1.15	10.3	−0.408	0
x_{mf}/z_0	27b	1.72	1.24	8.65	−0.746	0
Ar_f/z_0^2	27b	31.4	1.93	17.8	−0.642	1

TABLE VII

Validation statistics for the parameterisation of the passive scalar flux-source area model (FSAM), stable stratification (Equation 27a). For a description of the statistics used, see Table III

	a_f/z_0	e_f/z_0	d_f/z_0	x_{df}/z_0	x_{mf}/z_0	Ar_f/z_0^2
Number of runs (n)	32	32	192	32	32	192
Coeff. of determination (r^2)	1.0000	0.9999	0.9999	0.9999	0.9996	1.0000
Index of agreement (d)	1.0000	1.0000	1.0000	1.0000	0.9999	1.0000
rel. $RMSE_{tot}$ [%]	0.69	1.36	1.11	1.61	2.50	1.01
rel. $RMSE_{sys}$ [%]	0.02	0.56	0.32	0.80	0.84	0.32
rel. $RMSE_{unsys}$ [%]	1.69	1.24	1.06	1.40	2.36	0.96

which the five parameters in columns 3 to 7 refer. The form of Equation (27a) is used for all dimensions of both mini-SAM-2 and mini-FSAM in stable conditions, whereas (27b) provided good results in unstable conditions for all dimensions except a_c/z_0 of mini-SAM-2. Parameter α_5 is zero everywhere except for d/z_0 and Ar/z_0^2, where it is unity, in accordance with the linear dependence of these dimensions on σ_v/u_*.

Comparisons of the source area dimension parameterizations in mini-SAM-2

TABLE VIII

Validation statistics for the parameterisation of the passive scalar flux-source area model (FSAM), unstable stratification (Equation 27b). For a description of the statistics used, see Table III

	a_f/z_0	e_f/z_0	d_f/z_0	x_{df}/z_0	x_{mf}/z_0	Ar_f/z_0^2
Number of runs (n)	36	36	216	36	36	261
Coeff. of determination (r^2)	0.9996	0.9998	0.9990	0.9998	0.9862	0.9997
Index of agreement (d)	0.9999	1.0000	0.9998	0.9999	0.9965	0.9999
rel. $RMSE_{tot}$ [%]	2.03	1.43	3.14	1.59	14.1	3.21
rel. $RMSE_{sys}$ [%]	0.03	0.16	0.33	0.35	1.72	0.05
rel. $RMSE_{unsys}$ [%]	2.03	1.42	3.12	1.55	14.0	3.21

and mini-FSAM against the results of the respective full numerical models are presented in Figure 8a–d in composite scatter plots of all linear dimensions for stable and unstable conditions. The close agreement between the parameterizations and the full model results is also apparent in the validation statistics for each dimension presented in Tables III and IV for the scalar concentration-source area and in Tables VII and VIII for the flux-source area: the total standard difference between the two solutions amounts generally to less than 2% and the systematic portion of it remains typically far below 1%. For an explanation of the statistics used, see the footnote in Table III.

6. Summary and Conclusions

In this work, the surface source area of a turbulent diffusion measurement is defined in terms of the three-dimensional source-weight function (or footprint function). Source-weight functions for scalar concentrations and for scalar fluxes are presented based on the work of Horst and Weil (1992). The scalar concentration-source area model (SAM) published by Schmid and Oke (1990) is extended to include conditions of stable thermal stratification (SAM-2) and the parameterised statistical model is re-evaluated in normalised and thus more concise form (mini-SAM-2). In analogy to the scalar concentration-source area model, a scalar flux-source area model (FSAM) and its parameterized counterpart (mini-FSAM) are presented.

A comparison of the sensitivities of the source area dimensions for scalar concentrations and scalar fluxes showed that the source areas for fluxes tend to be smaller than the concentration-source areas by approximately an order of magnitude. This finding is important in applications where scalar fluxes over inhomogeneous areas are determined by mean profiles, the Bowen-ratio technique or other indirect methods relying on measurements of mean concentrations: the "field of view" of a concentration-sensor is much larger than that of a "flux-sensor" (e.g. an eddy-correlation instrument). This incongruity of the source areas may lead to consider-

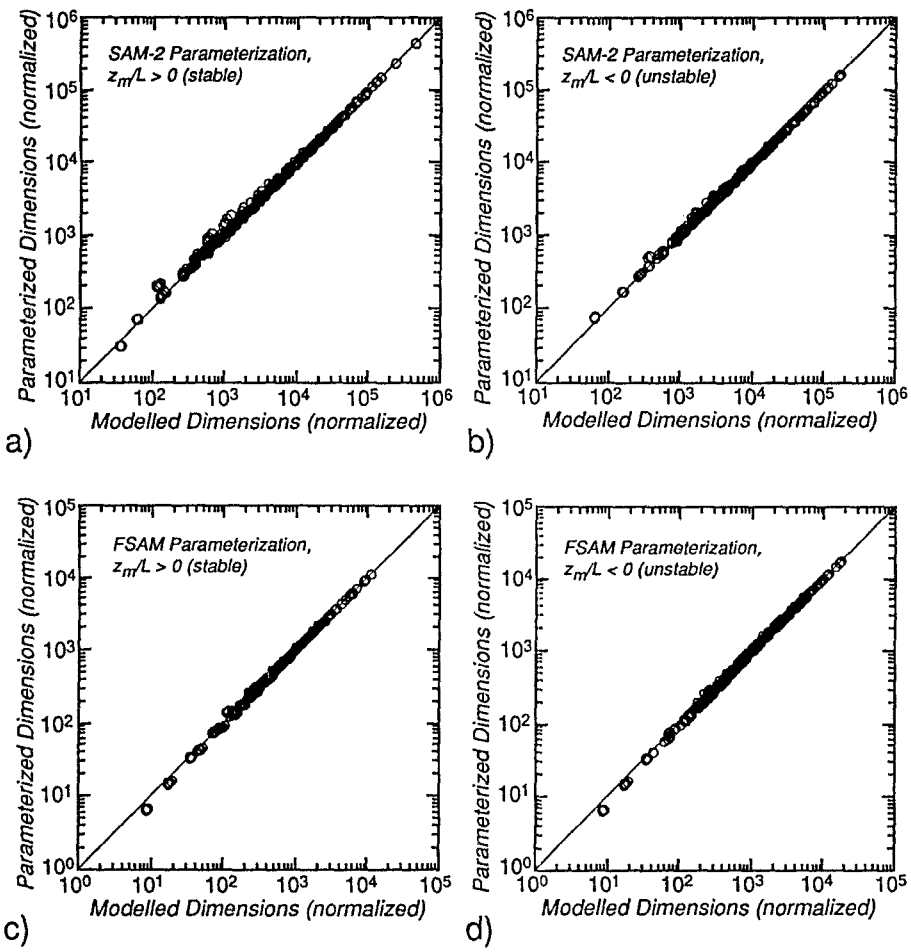

Fig. 8. Comparison of full numerical model results vs. parameterisation results of normalised source area dimensions. Composite scatter plots of all linear dimensions for (a) SAM-2 vs. mini-SAM-2 in stable conditions; (b) SAM-2 vs. mini-SAM-2 in unstable conditions; (c) FSAM vs. mini-FSAM in stable conditions; (d) FSAM vs. mini-FSAM in unstable conditions. The detailed validation statistics are presented in Tables III, IV, VII, and VIII.

able discrepancies between parameterized and actual fluxes in heterogeneous regions.

The qualitative response of the source area to changes in measurement height, thermal stability or crosswind turbulence, however, is very similar for fluxes and for concentration measurements. In summary, the effects of increasing stability and of increasing height are to elongate the source area and to move it farther upwind of the reference point, whereas the effect of increasing crosswind turbulence intensity is to enlarge the source area laterally. Thus, the implicit spatial representativeness of a scalar-concentration measurement (i.e., the degree to

which it reflects spatially averaged surface conditions; indicated by Ar/z_0^2) is strongly enhanced by increasing measurement height, and to a lesser extent by increasing stability and crosswind turbulence. The localness of the measurement (i.e., the degree to which it reflects local surface conditions; indicated by x_m/z_0), on the other hand, is decreased as a consequence of the same relationships.

This finding of a good qualitative agreement between SAM and FSAM confirms the conclusions of Schmid *et al.* (1991) about the (qualitative) stability dependence of the apparent spatial variability of turbulent flux measurements, although they used a scalar-source area model to approximate the flux-source areas.

With mini-SAM-2 and mini-FSAM, readily applicable tools are provided to estimate the surface area of influence of operational measurements. They combine the advantages of having nearly the same accuracy as the full numerical models that are based on boundary-layer diffusion theory with the convenience of a quick evaluation on a hand calculator.

Acknowledgements

The research leading to this paper was supported by grants from the Swiss National Science Foundation (≠ 20-29541.90) and the ETH-Research Fund. The author is indebted to Dr. Tom Horst of NCAR in Boulder, Colorado, for his constructive correspondence and to Drs. Tim Oke, Mathias Rotach and Martin Beniston for valuable comments on the manuscript.

References

Beljaars, A. C. M., Holtslag, A. A. M., and van Westrhenen, R. M.: 1989, *Description of a Software Library for the Calculation of Surface Fluxes*, Koninklijk Nederlands Meteorologisch Instituut, De Bilt, Technical Reports, TR 112, 32 p.

Gash, J. H. C.: 1986, 'A Note on Estimating the Effect of a Limited Fetch on Micrometeorological Evaporation Measurements', *Boundary-Layer Meteorol.* **35**, 409–414.

Gryning, S. E., Holtslag, A. A. M., Irwin, J. S., and Sivertsen, B.: 1987, 'Applied Dispersion Modelling Based on Meteorological Scaling Parameters', *Atmos. Environ.* **21**, 79–89.

Horst, T. W. and Weil, J. C.: 1992, 'Footprint Estimation for Scalar Flux Measurements in the Atmospheric Surface Layer', *Boundary-Layer Meteorol.* **59**, 279–296.

Horst, T. W. and Weil, J. C.: 1992, 'Application of the Flux Footprint to Scalar Flux Measurements within the Atmospheric Surface Layer', *Preprints, 10th Symposium on Turbulence and Diffusion*, Portland, Ore., Sept 29–Oct. 2, 1992, Amer. Meteorol. Soc., Boston, Mass., pp. 305–308.

Leclerc, M. Y., Finn, D., and Lamb, B.: 1992, 'Verification of the Source Footprint Model', *Preprints, 10th Symposium on Turbulence and Diffusion*, Portland, Ore., Sept. 29–Oct. 2, 1992, Amer. Meteorol. Soc., Boston, Mass., pp. 318–321.

Leclerc, M. Y. and Thurtell, G. W.: 1990, 'Footprint Predictions of Scalar Fluxes using a Markovian Analysis', *Boundary-Layer Meteorol.* **52**, 247–258.

Pasquill, F.: 1972, 'Some Aspects of Boundary Layer Description', *Q. J. R. Meteorol. Soc.* **98**, 469–494.

Pasquill, F. and Smith, F. B.: 1983, *Atmospheric Diffusion*, III Ed., J. Wiley & Sons, New York, 437 p.

Press, W. H., Flannery, B. P., Teukolsky, S. A., and Vetterling, W. T.: 1986, *Numerical Recipes: the Art of Scientific Computing*, Cambridge University Press, Cambridge, 818 p.

Schmid, H. P. and Oke, T. R.: 1990, 'A Model to Estimate the Source Area Contributing to Turbulent Exchange in the Surface Layer over Patchy Terrain', *Quart. J. Roy. Meteorol. Soc.* **116**, 965–988.

Schmid, H. P., Cleugh, H. A., Grimmond, C. S. B., and Oke, T. R.: 1991, 'Spatial Variability of Energy Fluxes in Suburban Terrain', *Boundary-Layer Meteorol.* **54**, 249–276.

Schmid, H. P. and Oke, T. R.: 1988, 'Estimating the Source Area of a Turbulent Flux Measurement over a Patchy Surface', *Preprints, 8th Symposium on Turbulence and Diffusion*, San Diego, Ca., April 26–29, 1988, Amer. Meteorol. Soc., Boston, Mass, pp. 123–126.

Schuepp, P. H., Leclerc, M. Y., McPherson, J. I., and Desjardin, R. L.: 1990, 'Footprint Prediction of Scalar Fluxes from Analytical Solutions of the Diffusion Equation', *Boundary-Layer Meteorol.* **50**, 355–374.

Van Ulden, A. P.: 1978, 'Simple Estimates for Vertical Diffusion from Sources near the Ground', *Atmos. Environ.* **12**, 2125–2129.

Willmott, C. J.: 1981, 'On the Validation of Models', *Phys. Geogr.* **2**, 184–194.

Wilson, J. D. and Swaters, G. E.: 1991, 'The Source Area Influencing a Measurement in the Planetary Boundary Layer: The "Footprint" and the "Distribution of Contact Distance"', *Boundary-Layer Meteorol.* **55**, 25–46.